The Construction of a Fully Integrated, MEMS Based, Atomic-Scale 3D Printer

Richard Lally, Matthias Imboden, Alexander Stange, Lawrence Barrett, Diego Pérez-Morelo and David J. Bishop, *Member, IEEE*

***Abstract*—We describe the construction of a fully integrated, MEMS based, 3D printer, capable of printing atomic-scale features. In this mm-scale device, we have built a complete nanofab for the manufacturing of nano scale devices and systems. The nanofab comprises surface micromachined MEMS, digitally programmable source of atoms; a stencil lithograpghy tool that uses a MEMS nanopositioner to determine where the atoms land; a substrate with on-chip leads for electrical characterization; a film thickness monitor; thermometer and heater. The device consists of three separate silicon die, flip-chip bonded to each other, forming a fully integrated, 3D system of systems. This device lets one build nano structures ranging from few atom structures up to micron scale devices. Applications range from searching for the Casimir Energy to the direct fabrication of quantum circuits, in situ, at cryogenic temperatures.**

***Index Terms*—Fab-on-a-Chip (FoC), flip-chip, MEMS, nanofabrication, quenched condensed thin films, Top-down approach**

I. Introduction

The field of nanomanufacturing endeavors to take research devices created in the laboratory and develop low cost, high volume ways to fabricate them. The discipline typically bifurcates into bottom-up and top-down approaches [1]-[4]. The bottom-up approaches are biologically inspired, with complex systems and organisms arising from a set of rules at the local level that allow the fundamental elements to self-assemble. While capable of creating systems of great complexity (human beings, for example), the rules are highly complex and our understanding of how to do this is only slowly emerging. This is a high entropy solution to the problem.

The alternative approach, based on how we manufacture integrated circuits, is top-down. In this approach, we have deterministic control over the structures and devices and completely specify what goes where and what it does. This approach endeavors to reduce the effects of entropy to zero, completely controlling where everything goes and minimizing the effects of randomness to as great an extent as possible. The current wave of 3D printers follows this top-down approach [5].

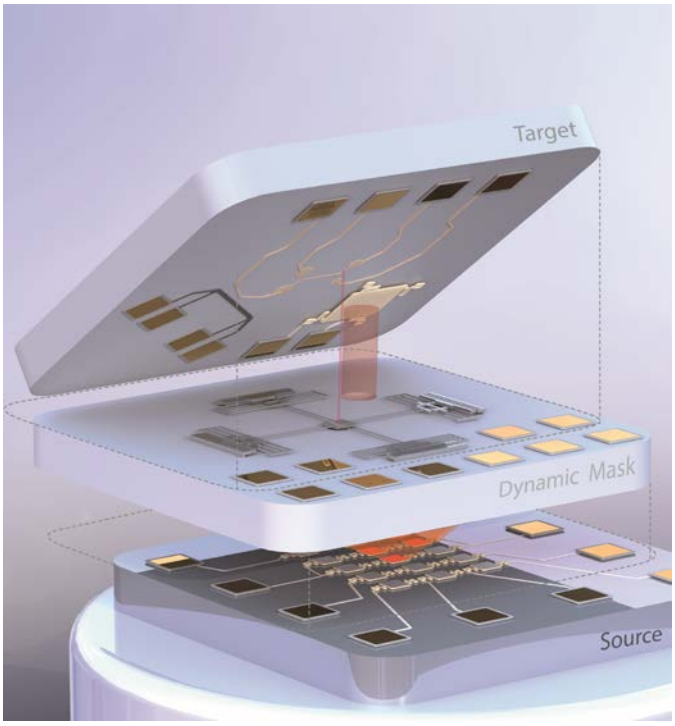

Fig. 1. Shown is the high level concept for our atomic scale, 3D printer. It consists of three layers, each a separate silicon die. The bottom layer is the atom source layer that emits the atoms for writing. The middle layer is the dynamic mask lithography tool that determines where the atoms land and the top layer is the target die upon which we write.

Manufacturing Science is being revolutionized by the development of 3D printing [6]. This technology allows for customized, high volume, low cost production of a wide range of objects and breaks the historical conundrum where one is forced to choose between custom/expensive or standardized/inexpensive.

Matter is composed of atoms and atomic-scale 3D printing is a universal and highly sought after goal by the researchers in

This work was funded by DARPA Atoms to Product (A2P) Program/Air Force Research Laboratory (AFRL) contract no. FA8650-15-C-7545 and by NSF Nanosystems Engineering Research Center for Directed Multiscale Assembly of Cellular Metamaterials with Nanoscale Precision: CELL-MET award ID: EEC-1647837.

Richard Lally, Matthias Imboden, Alexander Stange, Lawrence Barrett, are with the Division of Material Science, Boston University, Boston, MA 02215 USA (email: rlally@bu.edu; mimboden@bu.edu; stange@bu.edu; blawrenc@bu.edu).

Diego Pérez-Morelo is with the Instituto de Nanociencia y Nanotecnología (INN) Centro Atómico Bariloche, Comisión Nacional de Energía Atómica (CNEA) - CONICET, Argentina (email: diegojavierperez@cnea.gob.ar).

D. J. Bishop is with the Electrical and Computer Engineering Department, Physics Department, Division of Material Science, Department of Mechanical Engineering, Department of Biomedical Engineering, Boston University, Boston, MA 02215 USA (e-mail: djb1@bu.edu).

this field [7-9]. In this paper, we describe the construction of such an atomic-scale 3D printer as illustrated in conceptual rendering of Fig. 1. It comprises two basic technologies. The first, comparable to the conventional printer's extruder is a programmable atom source [10]-[12]. With it, we can extrude many different kinds of atoms in amounts from attograms to nanograms and in conjunction with nanometer apertures, lets us put the individual atoms we want onto a substrate when and where we want them. The second tool, comparable to the conventional printer's motion controllers, is a dynamic lithography system that aligns the atoms to where we want them on the substrate, as they are being evaporated [13]. It consists of a MEMS system of systems with multiple separately controllable micromotors. These two technologies form the basis of our Fab-on-a-Chip (FoC), a fully integrated MEMS-based nanofab that lets us do additive manufacturing at the atomic scale. It gives us deterministic, top down control, building circuits and structures with a few atoms at a time *in situ* at cryogenic temperatures [10].

The Holy Grail for 3D printing is the ability to deposit any atom, anywhere, anytime with high speed. Such a printer would allow one to build any structure or device one wishes, even metastable crystalline structures or molecules that do not naturally occur via normal kinetic pathways. This will enable additive manufacturing to move beyond building items we already know about and begin to explore structures that chemistry cannot produce.

II. Design

Actual images of our fully assembled printer are shown in Fig. 2. Visible are three separate silicon die that are flip-chip assembled to make the complete structure.

(a) (b)

Fig. 2. Optical images of NanoFab. (a) Image showing the scale of FoC. (b) Close up image of FoC.

The bottom layer is our programmable atom source [11]. With this source, we can thermally evaporate numerous metals in varying amounts, either concurrently or consecutively. The middle layer is our lithography tool. It determines where the atoms land. It consists of a MEMS plate with one or more apertures that is under the control of four electrostatic comb drives [14]. These motors move the plate in plane as the atoms pass through the backside of the die by way of a through wafer via. The position of the aperture(s) determines where the atoms land. The top chip is the target die. It consists of pre-positioned leads for in situ electrical measurements. The target die also contains a film thickness monitor, heater and thermometer for more refined metrology. Fig. 3a shows an actual printer, fully assembled with all three layers stacked together. As seen, the die are shifted relative to each other to allow for access to the leads for each layer. In Fig. 3a, the source die is on the bottom, the writing die in the middle and the target die on top. The leads for the target die are connected to pads on the writing die and those leads and the writing die leads are brought off chip via wire bonds on the middle die. The source die leads are also brought off chip directly to the wire bond pads seen on the lower layer. The schematic in Fig. 3c shows how the electrical connections are brought off chip for our system and the internal setup. Fig. 3b shows an optical micrograph of the assembled and packaged device. The package is a 20 lead, custom printed circuit board (PCB) with the height adjusted to allow for thermalization of experiments done at cryogenic temperatures. When the PCB is inserted into the cryostat the target die is in contact with the cold finger.

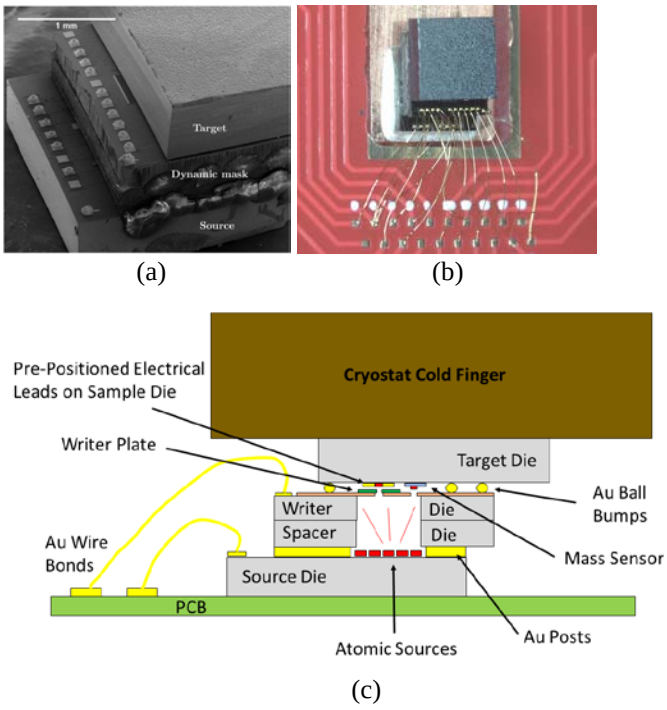

Fig. 3. Shown is the assembled nanofab. (a) SEM image of the three die, flip-chipped to form a single, integrated structure. (b) Packaged system with the wire bonds going from the stack of die to the custom PCB. (c) Shows a detail schematic of the FoC setup.

What we have done here is construct a system of systems. This approach is feasible because we use MEMS devices made in a foundry for all the elements discussed here [15]. The foundry model requires that their process be stable and that run to run, across an entire wafer, the devices we make are consistent and perform accordingly. This consistency allows us to design, build and optimize a specific element and then integrate it into a system with other elements, having a high degree of confidence it will perform as expected.

In what follows, we discuss each of the constituent layers separately: the source die, the writing die and the target die. Then we discuss integration of the three layers and finally, experimental results of the fully integrated system.

A. Atomic Source Die

The bottom layer of the object shown in Fig. 1 is our atomic source die. The concept of its operation is shown in Fig. 4. The device is a micron scale physical vapor deposition source. When heated, the atoms sublime or boil off the surface. Fig. 4a is a finite element model of the plate when tens of milliwatts of power are applied. The plate is fully suspended from the substrate and the experiments are performed in a vacuum, so the only cooling mechanism is via blackbody radiation, thermal conduction through the springs, and the evaporant. This cooling process keeps the plate temperature quite uniform, to within ~4 K [11]. The serpentine contacts to the plate are high resistance due to their geometry and so heat when a current is applied. They are serpentine in shape to minimize mechanical stresses caused by thermal expansion of the plate (see Fig. 4a-c).

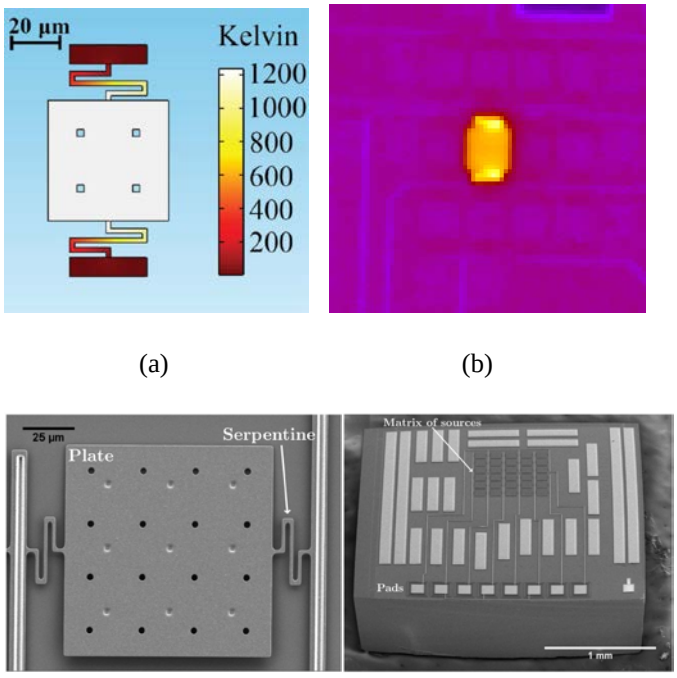

Fig. 4 Shown is the basic operating principle of our atom source. a) shows the Finite Element Model of the MEMS plate, suspended off the substrate, with a few tens of milliwatts of power applied. The central plate heats up to ~1200 K. [Reproduced from Ref. 11 with permission from the Royal Society of Chemistry.] b) shows a thermal camera image of an individual atom source among a matrix of sources. Notice surrounding sources remain at background temperature while the plate is ~800 K and the springs ~1000 K c) SEM image of a single source d) SEM image of source die and matrix of sources.

The atoms ones wishes to evaporate are prepositioned onto the source plates and boiled off due to its high temperature. In order to avoid forming a silicide with the atoms on the plate, the entire structure is coated using ALD with 20 nm of Al_2O_3. This coating forms a physically strong, chemically unreactive layer for our deposition surface. Fig. 4c shows an SEM image of a typical source plate (100 µm x 100 µm). The holes in the plate are to facilitate the release step of the MEMS device. Because of their small size, the thermal time constants of the atomic plates are quite short, typically a millisecond or so. This allows us to use pulse width modulation (PWM) to control the rate at which atoms leave the surface of the structure. These sources have been extensively characterized and the details are described in Ref. 10-12, 16. We have used these devices to evaporate In, Ag, Cu, Al, Pb, Fe, Sn and Au. Many other materials are possible. By varying the area of the source and using the PWM technique, one can puff off atoms in amounts ranging from attograms to nanograms. Fig. 4d shows a typical array of 30 sources used for the printer described here. The 5 x 6 array is divided into two groups so that two different metals can be evaporated separately or simultaneously. The sources in Fig. 4d are the dark grey squares near the center of the chip. The prominent white bars are spacers used to provide a standoff distance to protect the plates from the writer die above. The wire bond pads are the white squares on the bottom edge of the die. As shown in Fig.1, this die is placed on the backside of the writing die, with the 30 source plates directed towards the through wafer via.

B. Writer Die

Fig. 5a shows the front face of the writing die. It consists of a square (150 µm x 150 µm) plate, connected via eight tethers to

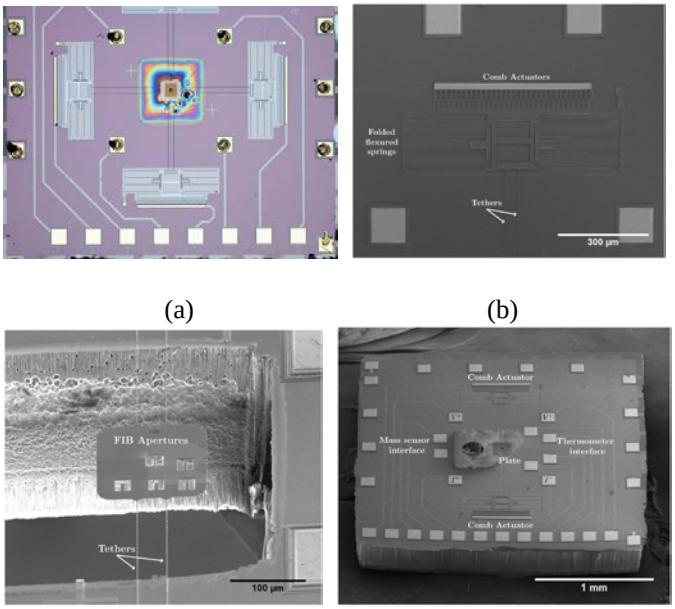

Fig. 5. Various images of different writer die. a) Optical image shows front side of the writing die with Au ball bumps. The writing plate is located over the through wafer via. The plate is connected to four electrostatic motors with 2 tethers for each motor. b) SEM image of electrostatic motor c) SEM image with FIB apertures shown above backside etch (BSE). d) SEM image of writer die with access holes and aperture created by FIB. Light colored squares are the gold bonding pads that align with target die pads.

four linear, electrostatic motors. One of the motors is seen in Fig. 5b and the writing plate is shown in Fig. 5c. As can be seen in Fig. 5a, the writing plate is located over a through wafer via [17], [18]. The through wafer via is marked by the interference pattern behind the writing plate. The atom source die is located on the backside of the writing plate and the atoms from the source pass through the via and the aperture(s) on the writing plate to land on the target die in locations determined by the position of the plate.

The four bonding pads that surround the writing plate are used to make contact with the target die that is mounted facing this side of the writing plate. The reason for this orientation is that for the finest patterns, the writing plate needs to be as close as possible to the substrate on which it writes.

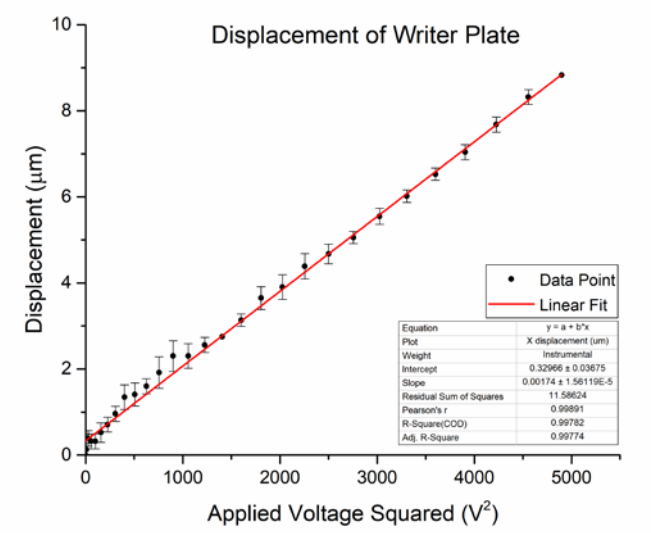

Fig. 6. Shown is the writer plate displacement as a function of the applied voltage squared. The expected V dependencies are also shown (red line) [20].

Apertures are milled into the writing plate using a FIB. Such apertures typically have sizes ranging from tens of nanometers to microns. Using a TEM on thin membranes, it is possible to create apertures with diameters less than a nanometer although we have not yet done this [19], [20]. For TEM aperture creation, the through wafer via will be crucial as the FIB works in reflection while the TEM works in transmission. Fig. 5c shows an example of five apertures cut into the writing plate with the FIB and the depth of the through via. Fig. 6 shows the X axis displacement of the aperture plate as a function of applied voltage squared. The expected quadratic behavior is observed and the Y axis displacement is similar [21]. There are various writer designs that offer different capabilities. Fig. 5d allows the interfaces necessary to connect the mass sensor and temperature sensor. Another configuration (not shown) provides 5 degrees of freedoms, which allows z axis adjustment to eliminate shadowing from source plates on the exterior of the array [22].

C. Target Die

A typical target die is shown in Fig. 7a. There are four leads which form a Van der Pauw geometry for resistance measurements [23]. The four contact pads at the corners of the cross make electrical contact to four similar pads on the writer die and are then led off chip to wire bonds. The deposited films are quite thin and so special care must be taken to produce leads that taper such that atomically thin films can make contact. Shown in Fig. 7b is our method for creating such contacts.

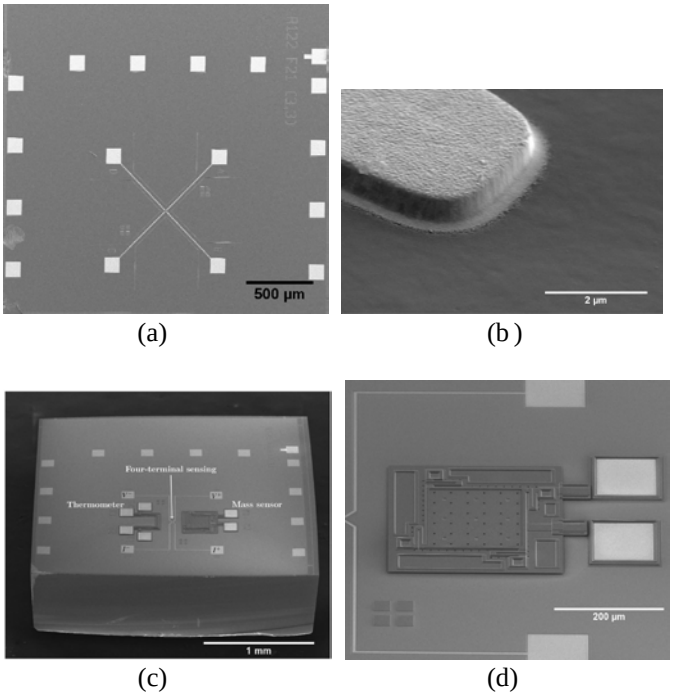

Fig. 7. SEM images of target die with sensors deposited on an insulating nitride layer. a) Shown is a typical target die with four electrical contacts in a Van der Pauw geometry. b) The end of our lead where a deposited film would make easier electrical contact. c) Image has mass sensor and temperature sensor added to the four contacts. d) Close up image of mass sensor.

This lead is fabricated by using the native PolyMUMPs gold placed on the nitride layer that has been thinned by outlining the lead with a dimple layer plus a Poly1/Poly2 Via contour. This produces a gold film whose edges bleed out onto the substrate making it easier for electrical contact to be made with atomically thin films on a smoother surface.

A typical target die would have electrical leads on it as shown in Fig 7a. However, other devices and structures can be added if needed. Shown in Fig. 7c is a target die with both a thermometer and a film thickness monitor. The film thickness monitor is a MEMS trampoline design shown in Fig. 7d [10], [24]. This device has a resonant frequency of ~80 kHz, a Q of ~50,000 and a mass sensitivity with 10 s averaging of ~2.5 fg, which corresponds to ~175 atoms/µm^2. The device is designed so that the springs, seen in the print through of the structure surrounding the 4-sided diaphragm, are shielded from the atoms landing on the surface. The unshielded atoms then change the mass of the plate and not the spring constant of the structure. Thus, as atoms land on the structure, its resonant frequency is reduced by an amount proportional to the added mass.

The thermometer shown in Fig. 8a consists of a polysilicon layer directly deposited onto the nitride substrate layer of the

PolyMUMPS process. It is a highly doped polysilicon layer that reduces the freeze out effect at cryogenic temperatures. Fig. 8b shows the resistance of this structure as a function of temperature. Using a conventional resistance bridge, we can resolve mK changes in temperature [10]. As depicted in Fig. 8b, the temperature sensor remains linear within the interested cryostat temperature range.

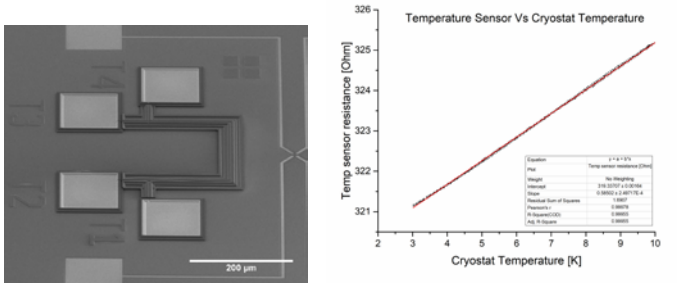

(a) (b)

Fig. 8. Temperature sensor image and data. a) Image of polysilicon temperature sensor on target die. b) Shown is the resistance of the thermometer presented in a) as a function of cryostat temperature. Typical resolution is ~1 mK.

III. Setup

A. Integration of the NanoFab

The three die described above, the atom source, writing plate and target die need to be processed, prepared and bonded to fully integrate the NanoFab die and create the Fab on Chip (FoC). This section describes the necessary steps to convert the die set as received from PolyMUMPs through the fully functioning assembly of the FoC. Each die will be addressed in this process.

B. Writer Die Preparation

In order to create the void for the metal to evaporate through from the atomic sources, a backside etch (BSE) process is performed on the writer die. First, the non-device side of the die is thinned to ~300 µm using a dicing saw. Next, a photoresist mask is patterned on the thinned side of the die and a Deep Reactive Ion Etch (DRIE) is performed where the native nitride layer of the PolyMUMPs process acts as a stopping layer. The die is then transferred to the FIB where a 95 µm hole is milled through the nitride layer at the bottom of the BSE under the writer plate. This produces an opening that allows access to the writer plate for the evaporant. Similarly, a 200 µm hole is milled through the nitride layer to allow access to the mass sensor. The aperture is then milled into the writer plate either from the top or bottom side of the die. Due to the depth of the BSE and difference between FIB and SEM images, it is more accurate and easier to mill the aperture(s) directly from the top of the writer die [17], [18].

To release the moveable structures, the sacrificial oxide layer is removed with hydrofluoric acid. After releasing the writer die, it is placed in a critical point dryer to reduce stiction between the plate/tethers and the nitride layer. Since the target die has no direct ball bonding pads to the PCB, all electrical connections are made through the writer die. To generate this electrical and structural connection between these two die, a gold ball bump is employed. Ball bumps (~ 90 µm diameter and ~ 12 µm height) are created using a ball bonder on each of the gold pads as seen in Fig. 5a and their wire tails removed.

C. Source Die Preparation

After releasing the source die, it is layered with 20 nm of Al_2O_3, as discuss previously. The source die is then loaded with the metal to be evaporated. This is done through Physical Vapor Deposition (PVD). In our case we use either thermal or electron beam deposition depending on the material being deposited. With the 5 x 6 array of sources one can deposit up to 1.5 µm of material on the source plates before the substrate and the plate begin to form a connection. For the information presented here, 1.0 µm of Pb was deposited onto the source die. During PVD deposition, the gold bonding pads are protected with a Ni shadow mask. This completes the source die preparation and the target does not need any preparation except for its release.

D. Assembly of NanoFab

The assembly of the NanoFab requires the use of a Flip Chip (FC) bonder. Since the writer die has the through via it cannot be picked up by the FC bonder since the vacuum would destroy the nitride layer and writer plate. Therefore, the target die is

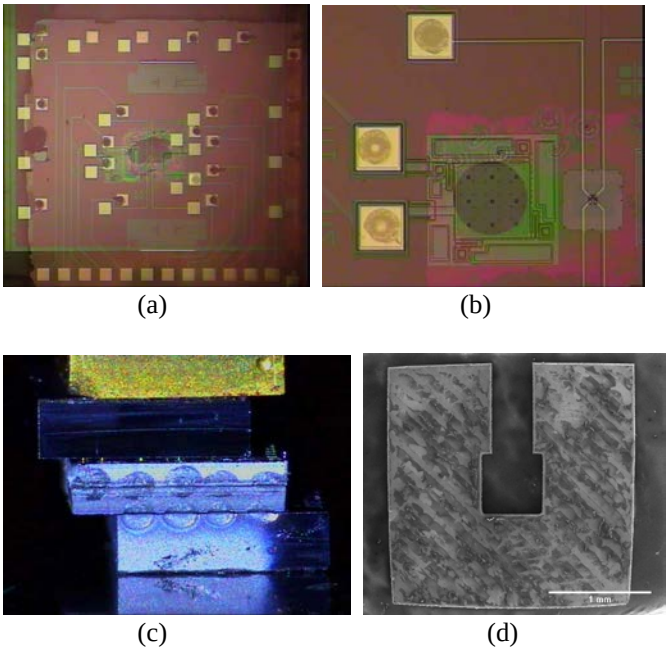

(a) (b)

(c) (d)

Fig. 9. Images of the NanoFab assembly process. a) Shown is a split beam image of the writer die and target being aligned. b) Fine adjustment is made to the alignment. Electrical leads are positioned beneath the aperture in the writer plate. c) Pictured is a side view of the FoC being flip chip bonded. d) SEM image of the spacer die which reduces shadowing effect.

picked up above the writer die and can be aligned with the split beam images to ~1 µm. Fig. 9a shows such an alignment being conducted. Each die has alignment marks, which aid in the coarse positioning. For fine alignment, the aperture of the writer plate is repositioned with respect to the leads on the target die as in Fig. 9b. After alignment, the two die are bonded by applying 20 N at 200 ˚C for 5 minutes as shown in Fig. 9c.

With a 5 x 6 array of atomic sources depositing over a distance of ~300 µm there will be some shadowing effect from the peripheral source plates. To reduce the shadowing effect, a spacer die can be added to increase the standoff distance. Here, we use roughly the same dimensions as the writer die (2.5 mm x 2.5 mm x 0.310 mm). Fig. 9d shows the spacer used for our results. The space has ~ 500 µm x 500 µm void created by the same BSE process. This opening aligns with the source array and the through via of the writer die. By including the additional ~300 µm spacer die it reduces the shadowing effect by half. The FC alignment is completed in the same manner as the target/writer die set for the remaining die. The two die are brought into contact with the spacer but no force or heat is applied. Since there is no electrical connection, a high viscosity cyanoacrylate glue is added to the sides of the die. This strongly adheres the individual die to each other but does not wick into the interior structure and interfere with the MEMS devices. If one looks carefully at the SEM image in Fig. 3a, one can see traces of the cyanoacrylate glue on the outside of the stack. The last die (source die) is then also FC aligned and attached. Again, the high viscosity glue is used instead of heating so that low melting point metals on the source plates are not affected. The assembled FoC is then electrically connected with ball bonds to the PCB and mounted in the cryostat.

IV. PERFORMANCE

When fully integrated, the system looks like the image shown in Fig. 2. Once all three die are aligned and bonded relative to each other, one has an integrated nanofab.

Shown in Fig. 10a is an example of a deposition at cryogenic temperatures as monitored by the mass sensor and the thermometer. Pb was deposited with 15 ms pulses turned on and off at 3 minute intervals. One can see that in the beginning, the rate of evaporation is high as the sources are full of Pb. However, as the deposition progresses, the amount of material per pulse decreases until the sources are exhausted. Note that the temperature increase during deposition is quite small, roughly 20 mK. This is a consequence of the nature of our source. The atoms leaving the atomic sources contain very little thermal energy. In a detailed study [12], we have shown that the atoms from our sources land on a substrate at cryogenic temperature with sufficiently little thermal energy that they do not form islanded structures as one normally finds. When the atoms land on a cryogenic substrate from our sources, they form disordered 2D films and do not ball-up. Thus, nanoscale structures stay nanoscale.

Fig. 10b is a graph of data from a typical FoC deposition using half of the 5 x 6 array of source plates. Here, atomic sources were loaded with ~1 µm of Pb before assembling the FoC. During this deposition, we increased the pulse width to 20 ms followed by a 2 second rest period. The pulse level was increased by 0.1 V every 30 seconds from 0 to 3.0 V. After 3.0 V the pulse level duration was increased to 1 minute for each 0.1 V increment. Also, depicted in Fig 10b is the cryostat sample temperature sensor and the FoC temperature sensor located on the target die. As expected, there is excellent correlation between the two sensors. Both show a sharp increase in temperature with the FoC temperature sensor being more responsive due to its proximity to the atomic sources. This increase, which peaks around the 1,500 seconds mark, is due to the evaporation of the Pb from the surface of the atomic plate springs. The atomic source plates resistance undergoes a

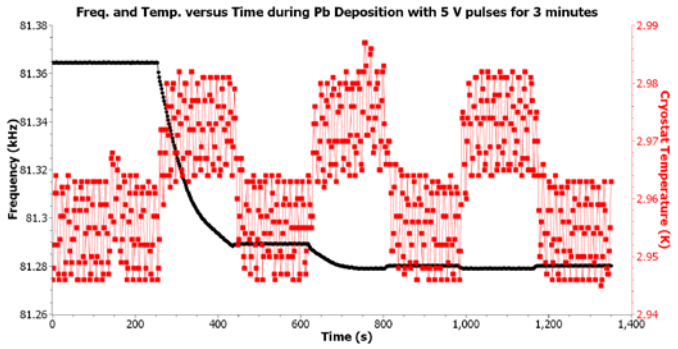

(a)

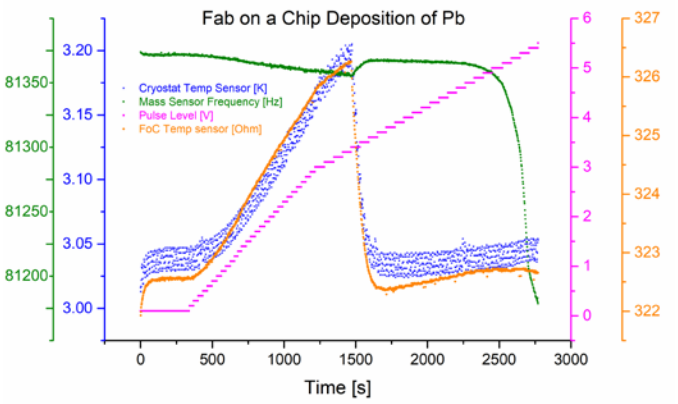

(b)

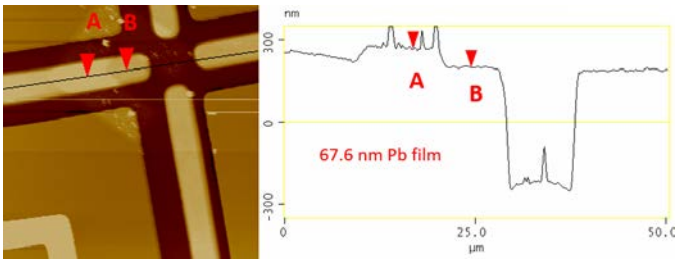

(c)

Fig. 10. Mass sensor and temperature sensor measurements. a) Measures of the deposited mass and temperature, using sensor shown in Fig. 7d, during a deposition of Pb using sources like those shown in Fig. 4d. b) Cryostat temperature, temperature sensor resistance, bias voltage, and mass sensor frequency graphed as a function of time for the deposition of Pb from 15 atomic sources. c) AFM recorded measurement of the Pb evaporated on target lead.

dramatic increase from ~14 Ω to ~170 Ω. At this point, there is an expected corresponding decrease in temperature. The mass sensor also shows a comparable reaction to the sharp increase and decrease in temperature due to the change in Pb coverage of the atomic sources. When the pulse level is ~ 4.6 V the Pb begins to evaporate, indicated by the decreasing frequency of the mass sensor.

For the FoC to be useful it must provide sufficient evaporated material to the target die. With the application of ~1 µm of Pb to the atomic sources this is possible. After fully depleting the atomic sources of Pb, AFM measurements were made on the target die. Fig. 10c shows that ~70 nm of Pb was deposited on the target die. Therefore, if using two different materials on half of the 5 x 6 atomic source array, ~35 nm of each material could be deposited simultaneously or consecutively. This is ideal for thin film applications.

It is possible to deposit more material on the target if necessary. A larger source plate has been developed which can be incorporated into the FoC [23]. Fig. 11a shows the 400 µm x 400 µm source plate and a spacer die has been attached using the FC bonder. A large slice of a Pb pellet can be positioned into the void of the spacer die (Fig. 11b) using a probe station. The alignment and assembly of the rest of the FoC remains the same and is seen in Fig. 11c. Using this setup with a 30 minute deposition, yielded ~3.5 µm of Pb on the target die. With this FoC setup, there is a wide range and amounts of deposited materials that can be achieved.

Another unique option is using the FoC without the target die attached. Here, the writer die can still be attached to the atomic source die and the two die setup can direct write onto other surfaces. Fig. 11d shows the setup, which allows customized application to fabricate nanoscale structures on fiber optics, metamaterials or other microscale devices.

Fig. 12 is an essential result of this paper. It shows the full functionality of our atomic scale, 3D printer. In Fig. 12 the LHS image shows the pattern of apertures on our writing plate. In the RHS the image displays the results of two depositions on the target die. First, the pattern in the LHS was positioned over the target die, the atomic sources were activated and the upper pattern in the RHS was produced. The sources were turned off, the writing plate was electrostatically repositioned ~1 µm, the sources were reactivated and the lower pattern was created. These in situ depositions were conducted with Pb at temperatures of ~3 K.

The target die leads were also tested as part of the FoC. Using the nitride layer and the writing plate as a mask, Pb was deposited through the aperture onto the four electrical leads (Fig. 13a). A four point resistance measurement was then conducted on the Pb sample. Fig. 13b shows a superconducting sample with a transition temperature of ~6.35 K. The superconducting transition temperature, resistance at 10 K and the mass sensor correlate to ~8.5 nm of deposited Pb. This result, as expected, differs significantly from the bulk Pb superconducting transition temperature of 7.19 K due to the thin layer deposited [12].

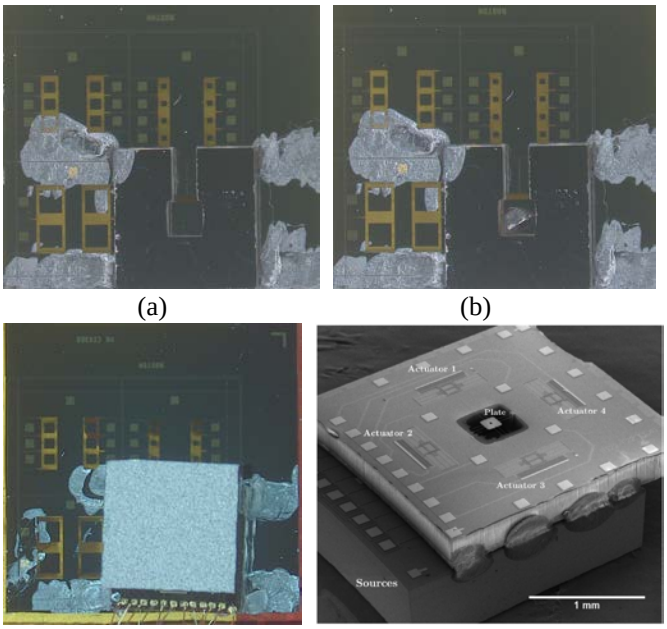

Fig. 11. Depicts alternative setups for increasing the deposition amount or patterning on other devices. a) Spacer die is attached over 400 µm x 400 µm source plate. b) Pb is loaded into the spacer die void and onto the source plate. c) Pre-bonded writer and target die is attached on top of the spacer die. d) Two die stack of source die and writer die shown for writing on other devices.

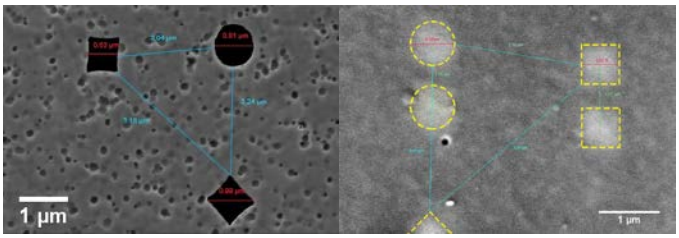

Fig. 12. Shown is the direct writing of a structure at ~3 K using FoC. The pattern of apertures in the writing plate is shown on the LHS of the image. The RHS shows two separate writing events. First, the upper structures were written, the source was turned off, the writing plate electrostatically repositioned and the lower set of figures were written. This was done in situ at cryogenic temperatures.

The atomic sources can also be used as heaters. Exhausted source plates or unloaded plates can be used to heat the target die. Fig. 13c shows the atomic sources being used to heat the Pb sample. The first two peaks show the Pb transitioning from being superconducting while the cryostat temperature remains at 3.1 K. Unlike the cryostat temperature sensor, the calibrated target die surface mounted temperature sensor indicates expected superconducting transition temperatures. In that next portion of Fig. 13c the temperature is being held on the shoulder of the superconducting transition by use of the heaters. Again, the proximity of the source die to the target when used as a heater allows very fine temperature changes. These fine adjustments can be made with 10 mV increments and/or 1 ms adjustments to the pulse width. This is a distinct advantage over the set point or heaters incorporated into typical cryostats.

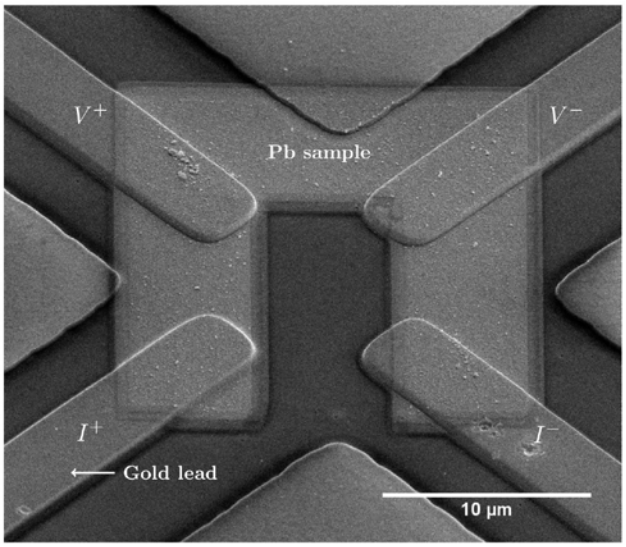

(a)

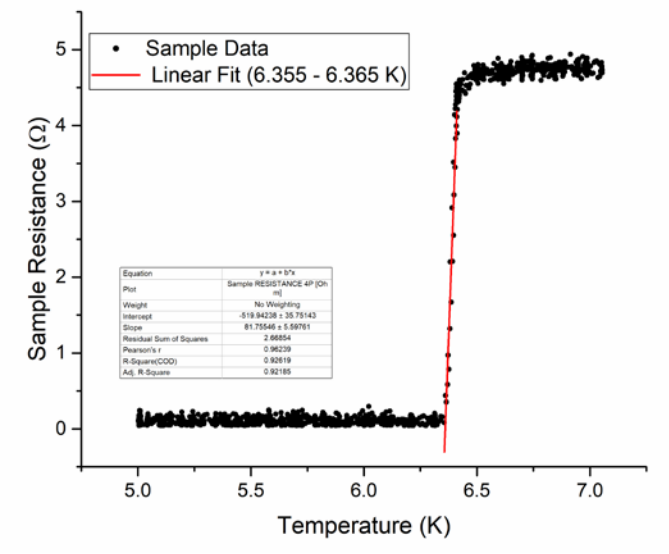

(b)

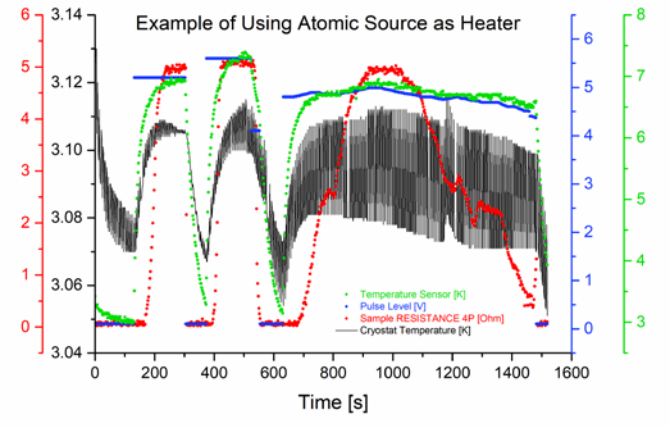

(c)

Fig. 13. Image and plotted results from Pb deposition with FoC. a) Pb deposited on Au leads for resistance measurements. b) Four point resistance measurement of deposited Pb showing a superconducting transition temperature of ~6.36 K. c) Graph shows how sources can be used to effectively control sample temperature with fine adjustments.

V. CONCLUSION

A couple of technologies allow our approach to be possible: the amazing advances in MEMS technologies that permit a writer plate to be positioned with sub-nanometer accuracy and the capability of FIBs and TEMs to mill silicon structures with nanometer scale apertures. The basic idea behind our device is that one can print with a stream of atoms by engaging one or multiple source plates while patterning the emission with the dynamic writer plate. There are many advantages to this approach: 1) One can deposit small amounts of atoms; (a) the thermal response time of the micrometer-sized sources allows for rapid start/stop action, (b) a responsive shutter can be incorporated to limit the number of atoms, and (c) the tens of nanometers sized aperture minimizes the number of atoms passing through. 2) Many control features and options for fast processing and unique structures are available; (a) arrays of apertures on the writer plate can fabricate many devices in parallel and (b) specifically sized and shaped apertures allows for the creation of novel structures with the dynamic patterning. 3) Multiple materials are capable of being deposited in situ; (a) conducting and nonconducting materials can be deposited to fabricate new structures and junctions and (b) because of these conducting and insulating materials, NEMS as well as electrical circuits are possible. 4) Due to the small footprint of the FoC, depositions can take place in specialized environments, such as a cryostat [10]. Consequently, the integrated NanoFab can address four important application areas. These include combinatorial materials science, direct printing of molecules, printing optical metamaterials with small numbers of atoms and in situ printing of superconducting Quantum circuits and Casimir energy experiments [16, 26 - 29]. Finally, and most importantly, as we show in Fig. 2, an assembled set of silicon die can contain all of the elements needed for an integrated nanofab.

In this paper, we described how we built a fully integrated, atomic scale 3D printer. By combining a source die, a writer die and a target die, one can construct a system of systems for doing both nanoscale research as well as high volume nanoscale manufacturing. Nothing prevents one from doing this at the wafer scale for a massively improved throughput. We believe this device allows for practical nanofabrication of single and few atom devices.

ACKNOWLEDGMENT

The authors would like to thank the Boston University's Photonics Center staff as well as Harvard University's Center for Nanoscale Systems staff for their ongoing assistance.

REFERENCES

[1] M. Imboden and D. Bishop, "Top Down Nanomanufacturing", Physics Today, vol. 67, no. 12, pp. 45-50 (2014).
[2] X. Zhang, C. Sun, and N. Fang, "Manufacturing at nanoscale: Top-down, bottom-up and system engineering", J. Nanoparticle Research, vol. 6, pp.125-130, (2004).
[3] B. Isaacoff and K, Brown, "Progress in Top-Down Control of Bottom-Up Assembly", Nano Lett., vol. 17, no. 11, pp. 6508-6510, (2017).

[4] D. Oh et al, “Top-down nanofabrication approaches toward single-digit-nanometer scale structures”, J. Mech. Sci, vol. 35, no. 3, pp. 837-859 (2021)
[5] H. Kodama, "Automatic Method for Fabricating a Three-Dimensional Plastic Model with Photo-Hardening Polymer", Review of Scientific Instruments, vol. 52, no. 11, pp. 1770-1773 (1981).
[6] K. Cummins, "The Rise of Additive Manufacturing", The Engineer, 5/24/2010,https://www.theengineer.co.uk/issues/24-may-2010/the-rise-of-additive-manufacturing/
[7] M. Imboden and D. Bishop, “Will It be Possible Someday to Build a Fab-on-a-Chip”, NanoWerk, 8/8/2013, http://www.nanowerk.com/spotlight/spotid=31758.php
[8] M. Berger, "Nanotechnology's Tiny Steps Toward Atomic-Scale 3D Fabrication", NanoWerk, 5/31/16, https://www.nanowerk.com/spotlight/spotid=43527.php
[9] S. Jesse, A. Borisevich, J. Fowlkes, A. Lupini, P. Rack, R. Unocic, B. Sumpter, S. Kalinin, A. Bellaninov, O. Ovchinnikova, "Directing Matter: Toward Atomic-Scale 3D Nanofabrication", ACS Nano, vol. 10, no. 6, pp. 5600-5618 (2016).
[10] M. Imboden, H. Han, T. Stark, E. Lowell, J. Chang, F. Pardo, C. Bolle, P. del Corro and D. Bishop, “Building a Fab on a Chip”, Nanoscale, vol. 6, no. 10, pp. 5049-5062 (2014).
[11] H. Han, M. Imboden, T. Stark, P. del Corro, F. Pardo, C. Bolle, R. Lally and D. Bishop, “Programmable Solid State Atom Sources for Nanofabrication”, Nanoscale, vol. 7, no. 24, pp. 10735-10744 (2015).
[12] M. Imboden, H. Han, T. Stark and D. Bishop, “Cryogenic Fab on a Chip Sticks the Landing”, ACS Nano, vol. 11, no. 9, pp. 8707-8716 (2017).
[13] M. Imboden, H. Han, J. Chang, F. Pardo, C. Bolle, E. Lowell and D. Bishop, “Atomic Calligraphy: The Direct Writing of Nanoscale Structures using a Micromechanical System”, Nano Letters, vol. 13, no. 7, pp. 3379-3384 (2013).
[14] R. Legtenberg, A. Groeneveld, and M Elwenspoek, “Comb-drive actuators for large Displacements” J. Micromech. Microeng., vol. 6, pp. 320–329. (1996)
[15] MEMSCAP Inc., http://www.memscap.com/products /mumps/polymumps/referencematerial
[16] Pérez-Morelo, Diego, Alexander Stange, Richard W. Lally, Lawrence K. Barrett, Matthias Imboden, Abhishek Som, David K. Campbell, Vladimir A. Aksyuk, and David J. Bishop. "A system for probing Casimir energy corrections to the condensation energy." Microsystems & nanoengineering 6, no. 1 (2020): 1-12.
[17] Stark, Thomas. "MEMS for Tunable Photonic Metamaterial Applications." PhD diss., Boston University, 2017.
[18] Barrett, Lawrence K. "Fab-on-a-chip: a MEMS approach to nanofabrication." PhD diss., Boston University, 2020.
[19] Storm, A. J., J. H. Chen, X. S. Ling, H. W. Zandbergen, and C. Dekker. "Fabrication of solid-state nanopores with single-nanometre precision." Nature materials 2, no. 8 (2003): 537-540.
[20] Van den Hout, Michiel, Adam R. Hall, Meng Yue Wu, Henny W. Zandbergen, Cees Dekker, and Nynke H. Dekker. "Controlling nanopore size, shape and stability." Nanotechnology 21, no. 11 (2010): 115304.
[21] J. Grade, H. Jerman, and T. Kenny, “Design of Large Deflection of Electrostatic Actuators”, vol. 13, no. 3, pp. 336-343, (2003).
[22] L. Barrett, T. Stark, J. Reeves, R. Lally, A. Stange, C. Pollock, M. Imboden and D. Bishop, “A Large Range of Motion 3D MEMS Scanner with Five Degrees of Freedom”, J. Microelectromech. Syst., vol. 28, no. 1, pp. 170-179 (2019).
[23] Oliveira, F.S., Cipriano, R.B., da Silva, F.T. et al., “Simple analytical method for determining electrical resistivity and sheet resistance using the van der Pauw procedure.” Sci Rep, 10, 16379 (2020). https://doi.org/10.1038/s41598-020-72097-1
[24] K. Park, N. Kim, D. Morisette, N. Aluru, and R. Bashir, “Resonant MEMS Mass Sensors for Measurement of Microdroplet Evaporation”, J. Microelectromech. Syst., vol. 21, no. 3, p. 702-711 (2012)
[25] L. Barrett , R. Lally, N. Fuhr , A. Stange , and D. Bishop, “A Chip-Scale, Low Cost PVD System”, J. Microelectromech. Syst., vol. 29, no. 6, pp. 1547-1555 (2020).
[26] Feliciano Giustino et al, “The 2021 Quantum Materials Roadmap”, J. Phys. Mater., 3 042006 (2020)
[27] Ludwig, A., “Discovery of new materials using combinatorial synthesis and high-throughput characterization of thin-film materials libraries combined with computational methods”, npj Comput Mater 5, 70 (2019). https://doi.org/10.1038/s41524-019-0205-0
[28] N. Litchinitser and J. Sun, “Optical meta-atoms: Going nonlinear”, Science, vol. 350, no. 6264, p. 1033-1034 (2015)
[29] Khoshnoud, Farbod, and Clarence W. de Silva. "Recent advances in MEMS sensor technology-mechanical applications." IEEE Instrumentation & Measurement Magazine 15, no. 2 (2012): 14-24.